Energy Consumption Modeling of Stereolithography-Based Additive Manufacturing Toward Environmental Sustainability

Yiran Yang,[1] *Lin Li,*[1] *Yayue Pan,*[1] *and Zeyi Sun*[2]

[1]*Department of Mechanical and Industrial Engineering, University of Illinois at Chicago, Chicago, IL, USA*
[2]*Department of Engineering Management and Systems Engineering, Missouri University of Science and Technology, Rolla, MO, USA*

Keywords:

design of experiments (DOE)
electricity consumption
environmental impact
industrial ecology
product surface quality
response optimization

Summary

Additive manufacturing (AM), also referred as three-dimensional printing or rapid prototyping, has been implemented in various areas as one of the most promising new manufacturing technologies in the past three decades. In addition to the growing public interest in developing AM into a potential mainstream manufacturing approach, increasing concerns on environmental sustainability, especially on energy consumption, have been presented. To date, research efforts have been dedicated to quantitatively measuring and analyzing the energy consumption of AM processes. Such efforts only covered partial types of AM processes and explored inadequate factors that might influence the energy consumption. In addition, energy consumption modeling for AM processes has not been comprehensively studied. To fill the research gap, this article presents a mathematical model for the energy consumption of stereolithography (SLA)-based processes. To validate the mathematical model, experiments are conducted to measure the real energy consumption from an SLA-based AM machine. The design of experiments method is adopted to examine the impacts of different parameters and their potential interactions on the overall energy consumption. For the purpose of minimization of the total energy consumption, a response optimization method is used to identify the optimal combination of parameters. The surface quality of the product built using a set of optimal parameters is obtained and compared with parts built with different parameter combinations. The comparison results show that the overall energy consumption from SLA-based AM processes can be significantly reduced through optimal parameter setting, without observable product quality decay.

Introduction

Additive manufacturing (AM) refers to an innovative manufacturing technique wherein the product is built by adding materials layer by layer, based on the three-dimensional (3D) geometry designed in computer-aided design (CAD) software (Huang et al. 2013). Attributable to this innovative capability, parts with complex geometries and customizable materials can

Conflict of interest statement: The authors have no conflict to declare.

Address correspondence to: Lin Li, Department of Mechanical and Industrial Engineering, University of Illinois at Chicago, 842 W Taylor Street, Chicago, IL 60607, USA. *Email:* linli@uic.edu; *Web:* http://smsrl.uic.edu/

DOI: 10.1111/jiec.12589
Editor managing review: Martin Baumers

Volume 21, Number S1

be fabricated through AM processes. Consequently, AM has gained significant public interest since it emerged in the 1980s, leading to a rapid proliferation of academic achievements and industrial applications in diverse industry subsectors, such as aerospace, health care, automotive, electronics, construction, etc. For instance, the Boeing Company builds more than 200 different parts using AM technologies for both military and commercial jets (Wohlers 2013). The National Aeronautics and Space Administration (NASA) also introduces AM processes into aerospace projects, for example, around 70 parts that make up the human-supporting Mars rover are built by AM processes (Stratasys 2015). According to the latest Wohlers Report, the AM industry, including all AM products and services worldwide, grew 25.9% (compound annual growth rate) to US $5.165 billion in 2015 (Wohlers 2016). Consequently, AM is poised to revolutionize the way products are designed, manufactured, and distributed (Gao et al. 2015).

The rapid growth of AM market is attributed to its distinguished advantages superior to traditional manufacturing processes. The most unique characteristic of AM is that it adopts a new production technique by adding layers of material, which eliminates the need for tooling, lubricants, and cutting fluids. This feature also implies the potential for a shorter product development cycle, easier process control, and higher product quality. Additionally, because the whole production process can be finished on one machine, regional and localized production can be incorporated into the AM process, leading to a shortened supply chain associated with lower energy consumption.

Attributable to the uniqueness of AM, multiple types of AM technologies have been developed to achieve differing production goals. Different AM processes can produce different types of materials by distributing and solidifying layers of materials in various methods (Wong and Hernandez 2012). Some processes build parts from powder material, for example, selective laser sintering (SLS), electron beam melting (EBM), binder-jetting (BJ), and laser powder forming. Some processes involve solid material similar to filament or wire such as fused deposition modeling (FDM). Additionally, some other processes, such as stereolithography (SLA) and Polyjet, produce parts from liquid resin by solidifying the liquid into solid through a light source. The diversity of current AM technologies facilitates continuous innovation and evolution and, consequently, will bring about more academic devotions and industrial utilizations.

Over the past few decades, numerous research efforts on AM have been dedicated to enhance the performance of different core techniques in AM processes, for example, laser technique (King et al. 2014) and curing process (Mitteramskogler et al. 2014; Lopes et al. 2014). The solidification methods (Yang et al. 2015b), geometry design approaches (Yang et al. 2015a), and computational algorithms (Martukanitz et al. 2014; Duro-Royo et al. 2015) have been widely investigated to improve the production procedure. Moreover, the product quality (Zha and Anand 2015), support structure (Hu et al. 2015), material properties (Park et al. 2014), and structure (Hong et al. 2015) have been studied to reveal the characteristics of parts built by AM processes. In addition to the technical research mentioned above, social impacts of the adoption of AM technologies have also been assessed (Huang et al. 2013). The occupational risk, economic analysis, and future challenges have been examined (Baumers et al. 2016; Weller et al. 2015).

Recently, attributed to the growing public concerns in climate change, more attention has been drawn to environmental sustainability related performance of AM processes considering energy, ecological, economic, and other aspects (Burkhart and Aurich 2015). Among the different perspectives, energy consumption of AM is considered as the top-driving factor that needs more academic studies, which is also identified as one of the unsolved issues for AM processes (Drizo and Pegna 2006; Short et al. 2015).

Several academic studies have been committed to the measurement of energy consumption of different AM processes. For example, the electricity consumed by the SLA system was acquired (Sreenivasan and Bourell 2009), the energy consumption for the BJ AM process was investigated (Xu et al. 2015), and the energy flow of the BJ AM process was monitored (Meteyer et al. 2014). Studies regarding energy consumption comparison between different AM processes as well as the comparison between AM and traditional manufacturing processes have also been conducted. For instance, a comparative assessment of the electricity consumption from two laser sintering (LS) AM machines was presented (Baumers et al. 2011a). In this research, the authors argued that LS energy consumption is mainly dominated by time-dependent energy consumption. In addition, case studies for three AM processes have also conducted: SLA, SLS, and FDM (Luo et al. 1999). For each type of AM process, the results of energy consumption differed with varying combinations of material types, equipment, and disposal scenarios. Further, the energy consumption for building nylon parts using SLS and injection molding (IM) processes were compared (Telenko and Conner Seepersad 2012). It was concluded that the SLS process consumed significantly more energy than the IM process; however, which can be partially offset by the energy contributed by the production of the injection mold from a life cycle viewpoint. Additionally, the energy consumption and environmental impacts among FDM, Polyjet, and traditional computer numerical control (CNC) processes were compared (Faludi et al. 2015). The researchers concluded that electricity usage had the dominant impact on the sustainability related performance for both AM process and traditional CNC process.

In addition to such research focusing on energy consumption measurement and comparison, a few studies on energy consumption modeling aiming to uncover the relationships between different parameters and energy consumption have been accomplished. For example, Mognol and colleagues (2006) investigated the influence of part orientation, layer thickness, support design, and manufacturing time on the energy consumption of three AM systems: Thermojet, FDM, and direct metal laser sintering. Kellens and colleagues (2014) presented parametric process models to estimate the environmental footprint

of the SLS process. More recently, Baumers and colleagues (2017) studied the relationship between geometry shape complexity and process energy consumption in EBM processes. They concluded that EBM does not show a strong association between shape complexity and energy consumption on a per-layer basis. Nonetheless, the current literature on energy modeling for AM processes is still limited and insufficient. Some types of popular AM processes (e.g., SLA) are barely considered for their energy consumption as a part of environmental sustainability performances. For SLA-based AM process, various parameters might influence the energy consumption, but have not been explored considering the different contribution of these parameters to the total energy consumption. Additionally, mathematical modeling for energy consumption is still lacking for AM processes.

To advance the state of the art of the research in energy consumption modeling of AM processes, this article is focused on mask image projection (MIP) SLA-based AM process, one of the most popular AM processes that can build parts by curing the liquid photopolymer resin layer by layer through an ultraviolet (UV) light source. The energy consumption model is established by quantifying the energy contributions of each subsystem of the MIP SLA-based AM machine. The design of experiments (DOE) method is used to guide the physical measurement to quantify the effects of various parameters on the overall energy consumption, explore the potential interactions between/among different parameters, optimize the combination of parameters to minimize the overall energy consumption, and validate the proposed energy consumption model. The potential greenhouse gases (GHGs) emission reduction attrubuted to the reduction of electricity consumption is also estimated.

The rest of this article is organized as follows. First, the mathematical model for the energy consumption of the MIP SLA-based AM process is established. After that, the experimental design and apparatus are introduced. Then, the experimental results are analyzed to validate the proposed mathematical model and optimize the combination of parameters to minimize the total energy consumption. Finally, the conclusion is drawn and the future work is discussed.

Energy Consumption Modeling

Mask Image Projection Stereolithography-Based Additive Manufacturing Process Illustration

The MIP SLA-based AM process has been mostly used in indoor environment as a desktop 3D printer. It has a faster production speed compared to other AM processes, contributed to by its innovative image projection method by exposing two-dimensional (2D) cross-section images instead of scanning them with a laser beam (Pan et al. 2012). Besides, it has the ability to produce a wide variety of shapes (Reeves 2009) while ensuring good quality and reasonable costs. Attributable to its unique process characteristics, the MIP SLA-based AM process has a great potential for energy efficiency improvement from several aspects. For example, layer thickness, curing time, and parameters associated with layer image can be configured in the building files. In addition, part orientation, position, and parameters regarding part geometry can also be adjusted in the control software.

As presented in figure 1, the MIP SLA-based AM process is comprised of a computer, a material tank with a transparent bottom, a building platform, a Z stage, a digital micromirror device (DMD), a UV light source, and a lens. All components are stationary during production process except the building platform that moves along the Z stage (in vertical direction), allowing the part being built on the platform layer by layer. The material tank contains liquid resin, which is solidified by the UV light source based on the layer image projected by the DMD. The entire production processes are divided into the following steps:

(1) The 3D geometry built in CAD software is imported into the control software and sliced into layers of 2D images with uniform layer thickness. Then, the control software generates the building files including all parameters the machine requires to build the designed part, such as material type, layer thickness, layer image, curing time, etc.
(2) After the building files are sent to the SLA machine, the building platform moves down to the liquid resin and touches the bottom of the material tank as the starting position before the actual building process.
(3) To start the production, DMD projects the first layer image on the bottom of the building platform through a transparent material tank so that UV light can cure this certain exposure area. During the UV curing process, the liquid resin transforms to a nontacky solid (Bajpai et al. 2002).
(4) After the first layer is solidified, the building platform moves up along the Z stage by the distance of layer thickness, preparing the new building surface for the next layer. Afterward, according to the building files, the DMD automatically projects the next layer image.
(5) Steps 3 and 4 are repeated until the part is finished. Then, the building platform moves up to its original position.

Energy Consumption Modeling

As illustrated in figure 2, the MIP SLA-based AM process contains multiple subsystems with their corresponding functionalities, that is, layer image projection, UV curing, building platform movement, lighting, and fan cooling. Each subsystem contributes different portions of energy consumption. Thus, it is critical to mathematically model the energy consumption for the overall production process as well as for each subsystem. Some subsystems with a minor contribution regarding energy consumption are not included in the mathematical model, such as layer image projection and lighting. Note that SLA-based AM processes do not rely on a heating subsystem.

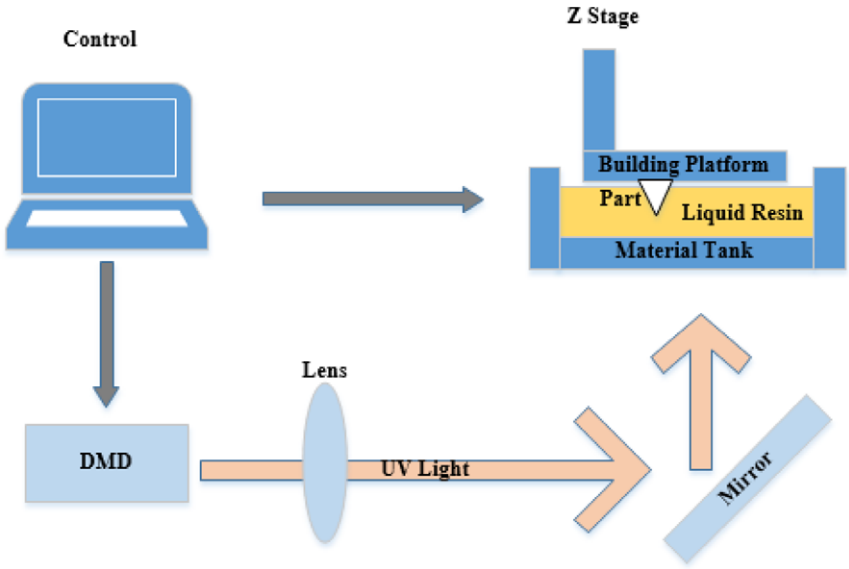

Figure 1 Mask image projection stereolithography-based additive manufacturing process diagram. DMD = digital micromirror device; UV = ultraviolet.

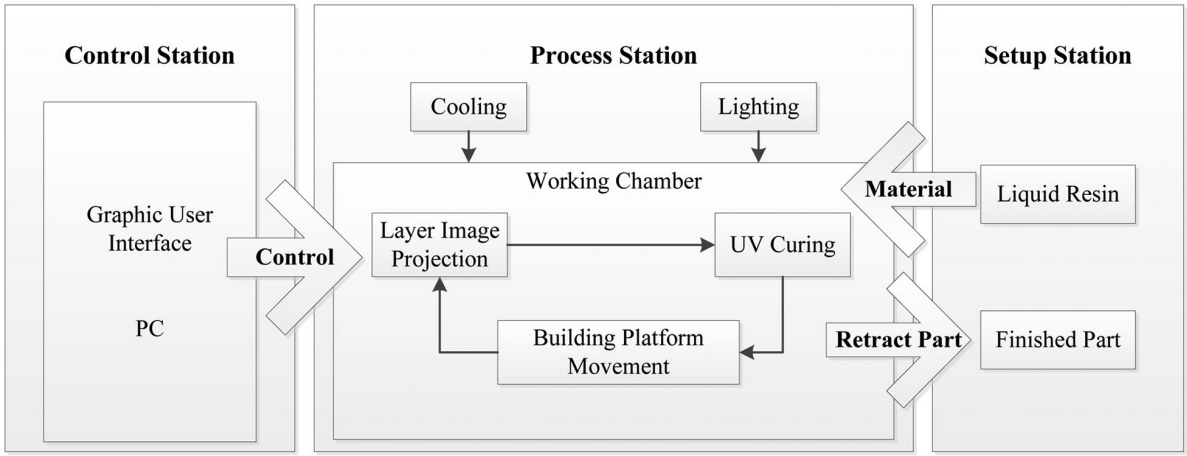

Figure 2 Mask image projection stereolithography-based additive manufacturing process subsystems illustration. PC = personal computer; UV = ultraviolet.

The energy consumption for each subsystem is modeled as follows:

(1) Energy Consumption of UV Curing Process

For certain part geometry with a total height of h and layer thickness of d, the number of layers K can be calculated through dividing h by d. For the ith layer, the UV curing energy consumption e_{curing} can be calculated as shown by equation (1):

$$e_{curing} = \frac{P_{UV} \times t_i}{a} \tag{1}$$

In equation (1), P_{UV} is the UV light source power output, and a is a constant determined by the UV source characteristics, which can be obtained by equation (2):

$$a = \eta_1 \times \eta_2 \times \eta_3 \tag{2}$$

where η_1, η_2, and η_3 are the lighting efficiency, ratio of effective wavelength over the total wavelength, and material absorptivity for a specific UV source, respectively. They can be obtained from machine documentation.

In equation (1), t_i is the curing time for the ith layer, and it can be calculated by equation (3).

$$t_i = \begin{cases} t_1 & i \in [1, i_b] \\ t_1 - s \times (i - i_b) & i \in [(i_b + 1), i_t] \\ t_2 & i \in [(i_t + 1), (h/d - 3)] \\ t_1 & i \in [(h/d - 2), (h/d)] \end{cases} \tag{3}$$

Table 1 Description of experimental control parameters

Symbol	Control parameter	High level (+1)	Low level (–1)	Center point
A	Layer thickness d (mm)	0.05	0.025	0.0375
B	Curing time for stable layers t_2 (s)	6.5	4	5.25
C	Curing time transition rate s (s/layer)	2.7	1.125	1.9125
D	Orientation	90°	0°	45°

Note: The detailed definitions of factors *B* and C can be found in equation (3).
mm = millimeters; s = seconds.

Table 2 Energy consumption results comparison with current literature

Case no.	AM process	Material	Capacity utilization (%)	Layer thickness (mm)	Specific energy consumption (kWh/kg)	Reference
1		PA2200	3.41	0.12	39.20	
2	SLS	PA2200	3.02	0.15	40.30	(Kellens et al.
3		PA3200	2.50	0.15	36.00	2014)
4	SLS	Polymer	/	0.15	40.1	
5	SLA	Epoxy resin	/	0.15	32.47	(Luo et al.
6	FDM	ABS	/	0.4	115.20	1999)
7	SLA	LS600M	0.05	0.025	175.95	This research

Note: AM = additive manufacturing; SLS = selective laser sintering; SLA = stereolithography; FDM = fused deposition modeling; mm = millimeters; kWh = kilowatt-hours; kg = kilograms.

Equation (3) describes the relationships between curing time and the layer that is being processed. From the first layer to layer i_b, the curing time is t_1. t_1 is usually longer than solidification needs, in order to ensure that several layers at the beginning can be fully cured. Starting from the layer (i_b+1), curing time decreases from t_1 to t_2 with a linear rate s (seconds per layer) until layer i_t. Thus, layers from (i_b+1) to i_t are defined as "transition layers" because of the transition of curing time from t_1 to t_2. After that, the curing time maintains at the value of t_2 for the layers from (i_t+1) to (h/d-3). These layers are defined as "stable layers" because they have uniform curing time. The curing time for the last three layers changes back to t_1 to ensure that the part is fully cured with good quality.

Thus, the total energy consumption of UV curing for all the K layers can be calculated as shown by equation (4).

$$E_{curing} = \sum_{i=1}^{K} \frac{P_{UV} \times t_i}{a} \tag{4}$$

(2) Energy Consumption of Building Platform Movement

During the production process, the material tank maintains the same position all the time, while the building platform moves along vertical direction (Z stage). An electric stepper motor provides power for the vertical movement of the building platform, and its power output is represented by P_m. The energy consumption of this movement can be calculated by equation (5).

$$E_{platform} = \sum_{i=1}^{K} (P_m) \times t_i \tag{5}$$

(3) Energy Consumption of Cooling System

The energy consumption of cooling system can be calculated by equation (6):

$$E_{cooling} = P_{cooling} \times t_{cooling} \tag{6}$$

where P_{heater} is the power output of cooling fan. $t_{cooling}$ is the cooling time which is slightly longer than the production time.

Thus, the total energy consumption can be obtained by equation (7).

$$E_{total} = E_{curing} + E_{platform} + E_{cooling} \tag{7}$$

Experimentation

Experiment Design Methodology

The mathematical model of energy consumption is established by modeling the energy consumption contributed from each subsystem of the MIP SLA-based machine. Different parameters, such as the number of the layers and curing time, are integrated into the energy consumption of these subsystems. However, we do not have the knowledge of whether or not the interactions between different parameters exist. The interaction between different parameters means that the response of the energy consumption may be different when changing one parameter while keeping other parameters at different levels. For example, if the curing time is changed from a lower value to a higher value at the different levels of the layer thickness, the energy consumption could be maintained as the same or change along the way.

Table 3 Factorial design analysis results

Factor	*Sum of squares*	*p value*
A	2.12e11	0.000
B	5.83e9	0.000
C	2.20e6	0.556
D	6.27e9	0.000
*A*B*	1.41e8	0.000
*A*C*	9.89e5	0.692
*A*D*	3.29e8	0.000
*B*C*	1.37e7	0.150
*B*D*	7.95e7	0.002
*C*D*	6.78e7	0.004
*A*B*C*	4.38e7	0.015
*A*B*D*	2.27e8	0.000
*A*C*D*	3.82e5	0.805
*B*C*D*	5.80e7	0.006
*A*B*C*D*	1.38e7	0.640

To find such interactions, multiple runs of experiments with different combinations of input parameters need to be implemented. The DOE can provide the smallest number of runs in which the influences of a given number of input parameters on the response can be studied. It is more efficient than the one-factor-at-a-time strategy (Montgomery 2012). Therefore, in addition to the mathematical model of energy consumption, the DOE is also used to design the experiment with different combinations of the input parameters so that the interactions between different parameters can be examined, the optimal parameter setting to minimize the energy consumption can be identified, and the mathematical model can be validated. The detailed configurations of the experiment designed by the DOE are illustrated as follows.

A two-level factorial design is used to establish the experiments including four controllable factors (or input parameters), that is, layer thickness (d), curing time for stable layers (t_2), curing time transition rate (s), and orientation as shown in table 1. The first three factors are process-related factors, whereas the last one is a geometry-related factor. Two levels, that is, low and high, for each factor, as shown in table 1, are considered. Two replicate experiments are conducted for each possible combination of all four factors with different levels. Moreover, four center points are added to the experiment design to provide a measure of process stability and inherent variability and to check for curvature. A 2^4 factorial design combined with four center points result in a total 36 experiment runs.

For the MIP SLA-based AM machine in the experiments, the default value for layer thickness is 0.025 millimeters (mm), with a higher level of this parameter set as 0.05 mm. Curing time for stable layers originally is 6.5 seconds, and a lower level of 4 seconds is also investigated. As for the transition rate from longer curing time to shorter curing time, both default 1.125 seconds per layer and a higher level of 2.7 seconds per layer are studied. The orientation is also considered for initial value 0° and higher level of 90°.

These four input factors are coded as +1, –1, and 0 in Minitab, where +1 denotes the high level; –1 denotes the lower level; and 0 denotes the center point. Coded variables are used to ensure that factors with different numerical value scales can be compared to determine the significance of the factors' impact on the response, in this case, the overall energy consumption.

Experiment Apparatus

The MIP SLA-based AM machine used for the purpose of experimentation is a Perfactory Micro EDU 3D printer. It is the smallest desktop 3D printer in size with the highest resolution of 150 microns (μm) for the XY axis and 50 to 100 μm for Z axis (EnvisionTEC 2015). Equipped with state-of-the-art direct light projection technology from Texas Instruments, it can achieve a precise layer image projection by DMD. The light-emitting diode UV light source is used for the curing process, solidifying the liquid resin to solid form. With all mentioned advanced machine specifications, this 3D printer can achieve a fast building speed up to 20 mm/hour for full building capacity (100*75*100 mm). In addition, seven types of materials can be built through this AM machine, including LS600 M (used in the experiments), HTM140 M, ABS Tough M, E-Denstone M Ivory, E-Denstone M Tough, ABS Flex M, and Superflex M.

The measurement equipment is the single clamp-on power meter CW10 by Yokogawa, with a maximum alternating current/direct current (AC/DC) current 600 angstroms and maximum AC/DC voltage 1,000 volts. It can also measure power factor, frequency, resistance, etc. The measured data were recorded every 5 seconds.

Attributable to the existence of power factor, the current and voltage data obtained from the power meter aforementioned cannot be directly used to calculate the electricity consumption. Because the Perfactory Micro EDU 3D printer adopts a single-phase power supply, its power factor can be measured by the wattmeter-ammeter-voltmeter method (Prasanna Kumar et al. 1995), and thus the real power consumption $P_{real\ power}$ can be calculated as shown in equation (8):

$$\begin{aligned} P_{real\ power} &= power\ factor \times S_{apparent\ power} \\ &= power\ factor \times (U_{measured} \times I_{measured}) \end{aligned} \quad (8)$$

where $S_{apparent\ power}$ stands for the apparent power calculated using measured voltage $U_{measured}$ and current $I_{measured}$. Test runs are conducted to obtain the power factor of the system, which turns out to be 0.85.

Results

Base Case Results Using Default Condition

Under the default working conditions (i.e., layer thickness 0.025 mm, curing time for stable layers 6 seconds, curing time transition rate 1.125 seconds/layer, and orientation 0°), the measured energy consumption is 278,707.35 joules (J) for building a bolt with 1 centimeter of height. The absolute

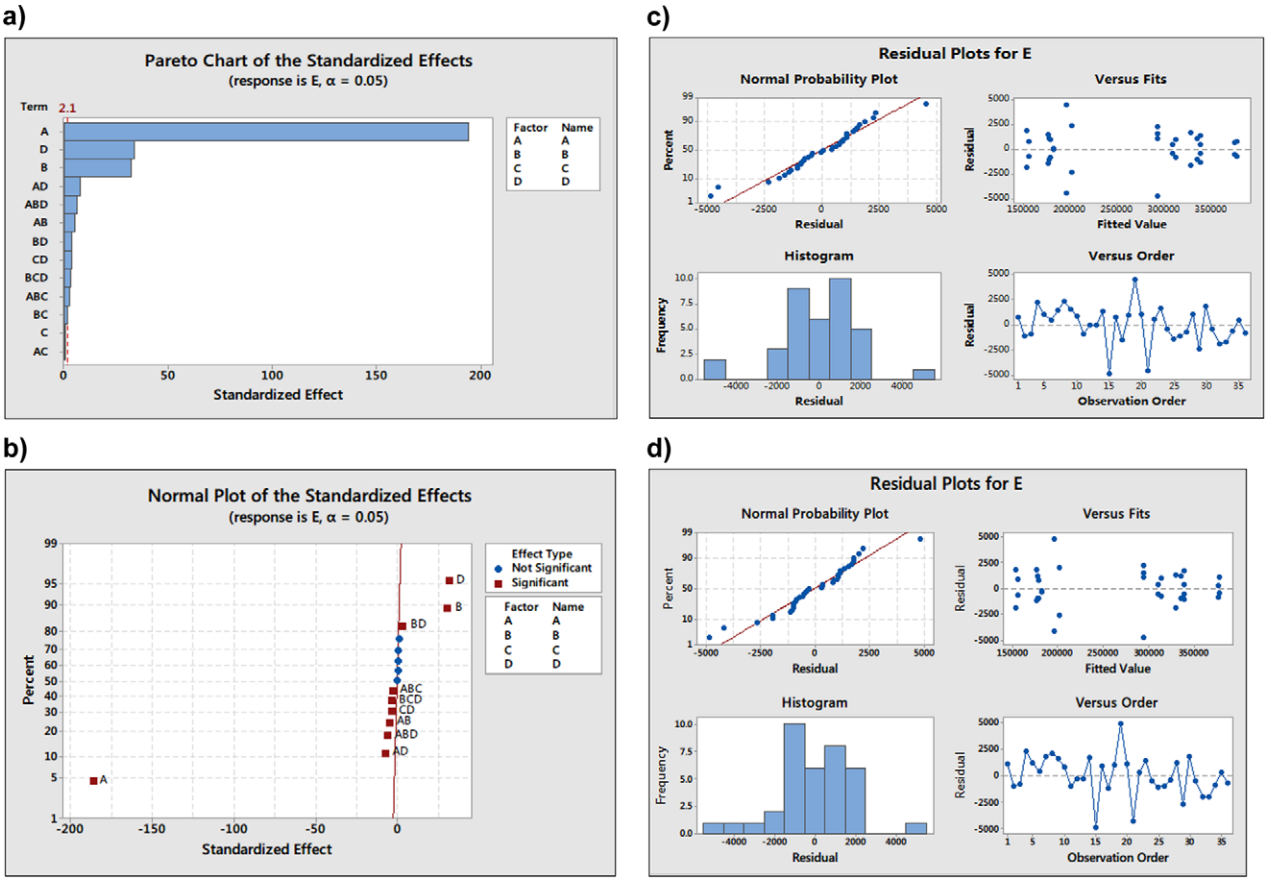

Figure 3 Factorial analysis results and model adequacy checking. (a) Pareto chart; (b) normal plot; (c) adequacy checking for factorial design model; (d) adequacy checking for refined statistical model.

percentage error compared to the calculated result using the proposed mathematical model (264,531.672 J) is only 5.36%. The difference may come from the use of rated power of each subsystem provided by machine documentation rather than the actual power for the calculation using the mathematical model. The actual power output from each subsystem cannot be obtained, because of the limitations of the measuring equipment and the complexity of the subsystems. Therefore, the power rating acquired from machine documentation is used for approximate calculation, leading to the error.

The measurement results based on the default condition are also compared with some other processes in existing literature as listed in table 2.

In table 2, Kellens and colleagues (2014) investigated the SLS process through experiments using three types of materials with different layer thicknesses. Luo and colleagues (1999) compared three AM processes: SLS, SLA, and FDM, and they found that FDM has the largest energy consumption. The energy consumption from our results using the default configuration (case no. 7) is relatively higher than the results in the literature. Three main reasons are considered as follows. First, different types of AM processes adopt diverse manufacturing technologies and produce dissimilar types of material, thus they might possess different energy consumption characteristics. Second, the capacity utilization (the ratio of printed part volume and the maximum building volume provided by the AM machine) also influences the specific energy consumption. According to Baumers and colleagues (2011b), a lower capacity utilization possibly leads to larger specific energy consumption (SEC) for some types of AM processes. Compared with a 2.50% to 3.41% capacity utilization ratio from Kellens and colleagues (2014), the lower capacity utilization ratio in this research is another probable reason why the SEC from this research is high. Third, the layer thickness in our research is much smaller than the others, leading to better product quality as well as higher energy consumption.

Factorial Analysis Results

The experimental results are imported to Minitab to conduct further factorial analysis with a significance level of 0.05 and to obtain the statistical model. According to the factorial analysis results shown in table 3, factors A, B, D, and interactions A*B, A*D, B*D, C*D, A*B*C, A*B*D, B*C*D are of great significance, and factor C, and interaction A*C, B*C, A*C*D, A*B*C*D lack significance. Factors A, B and D have a substantial effect on the response attributed to their direct influence on production time, which is also the reason for the

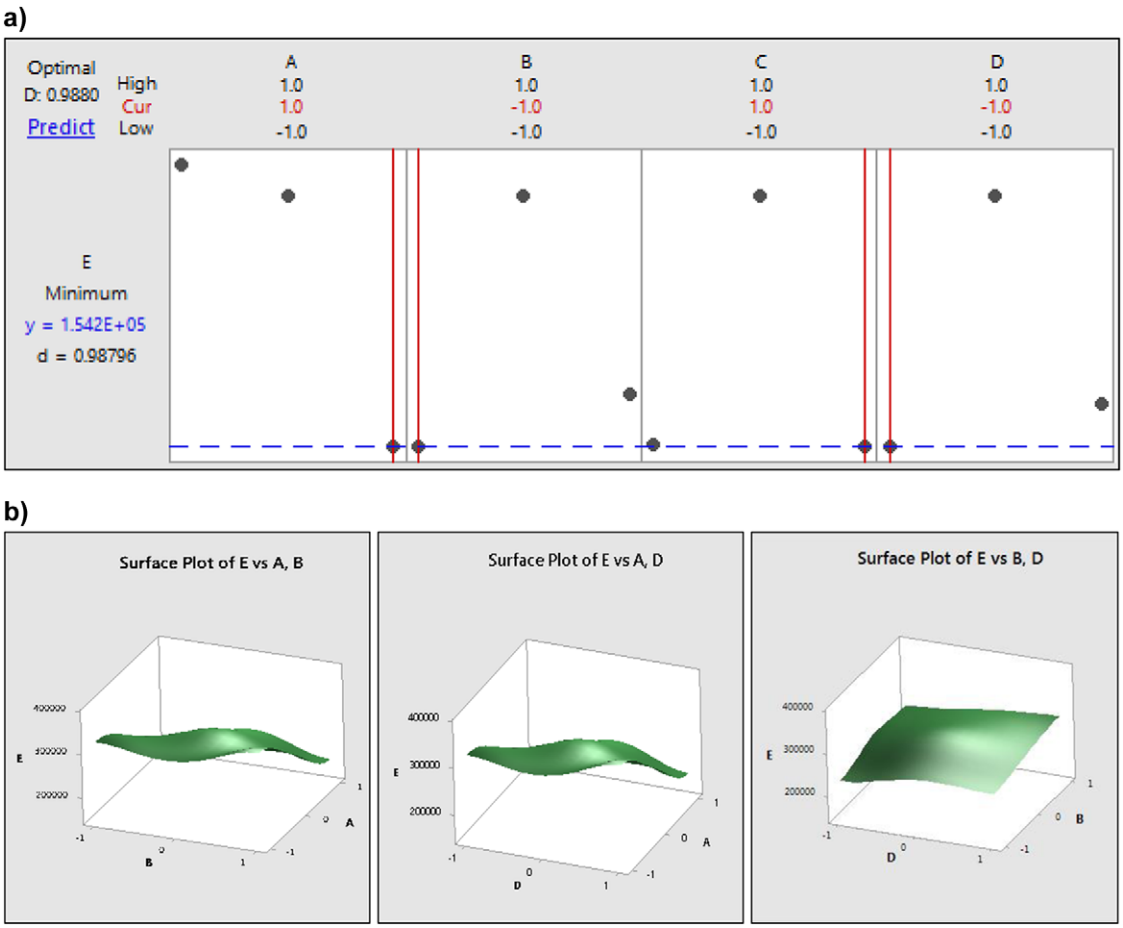

Figure 4 Response optimization results and surface plots. (a) Response optimization results; (b) surface plot of E versus A and B, A and D, B and D. Cur = current.

high significance of interactions between these three factors. Although factor C also affects the production time, it only lasts for a very short period (usually 25 layers). Therefore, the effects from factor C is negligible. Based on the DOE results, even though factor C and other related interactions, such as A*C, B*C, A*C*D, and A*B*C*D, are not significant, interactions C*D, A*B*C and B*C*D have substantial effects. From the observations of the SLA production process, the duration of factor C changes with factor D, where C lasts longer when the part is built horizontally and shorter when the part is built vertically. Therefore, the interaction between factors C and D is important. In addition, three-order interactions A*B*C and B*C*D are significant because of the similar reasons where factor C changes according to the changes of factor A and B and factor B and D.

The Pareto chart of the standardized effects is shown in figure 3a, and the normal plots of the standardized effects are shown in figure 3b. It can be seen that factor *A* has a negative impact on the output *E* (total energy consumption), whereas factors *B* and *D* have a positive impact on the output *E*. The interaction terms of *AD*, *ABD*, *BD*, *CD*, *BCD*, *ABC*, and *BC* have relatively minor influence on the output *E*, whereas factor C and interaction *AC* have basically ignorable effects.

The model adequacy is checked as shown in figure 3c. The normality (plus histogram) plot and the plot of residuals versus observation order illustrate that the residuals are normally and independently distributed. The plot of residuals versus fitted value verifies that the assumption of constant variance is satisfied.

The corresponding refined statistical model can be written as:

$$\begin{aligned} E &= 259,101 - 81,321A + 13,492B + 13,993D - 2096A \\ &\quad \times B - 3207A \times D + 1576B \times D - 1456C \\ &\quad \times D - 1170A \times B \times C - 2662A \times B \times D - 1346B \\ &\quad \times C \times D + 34,970CtPt \end{aligned}$$

where *CtPt* is the center point. The regression model adequacy check is shown in figure 3d.

Based on the factorial analysis, the optimal levels of the input factors that can lead to minimized energy consumption are identified using the response surface method as shown in figure 4a. A higher level of factor A, and lower level of factors *B* and *D*, would lead to minimized energy consumption of this MIP SLA-based AM process. In addition, figure 4b illustrates

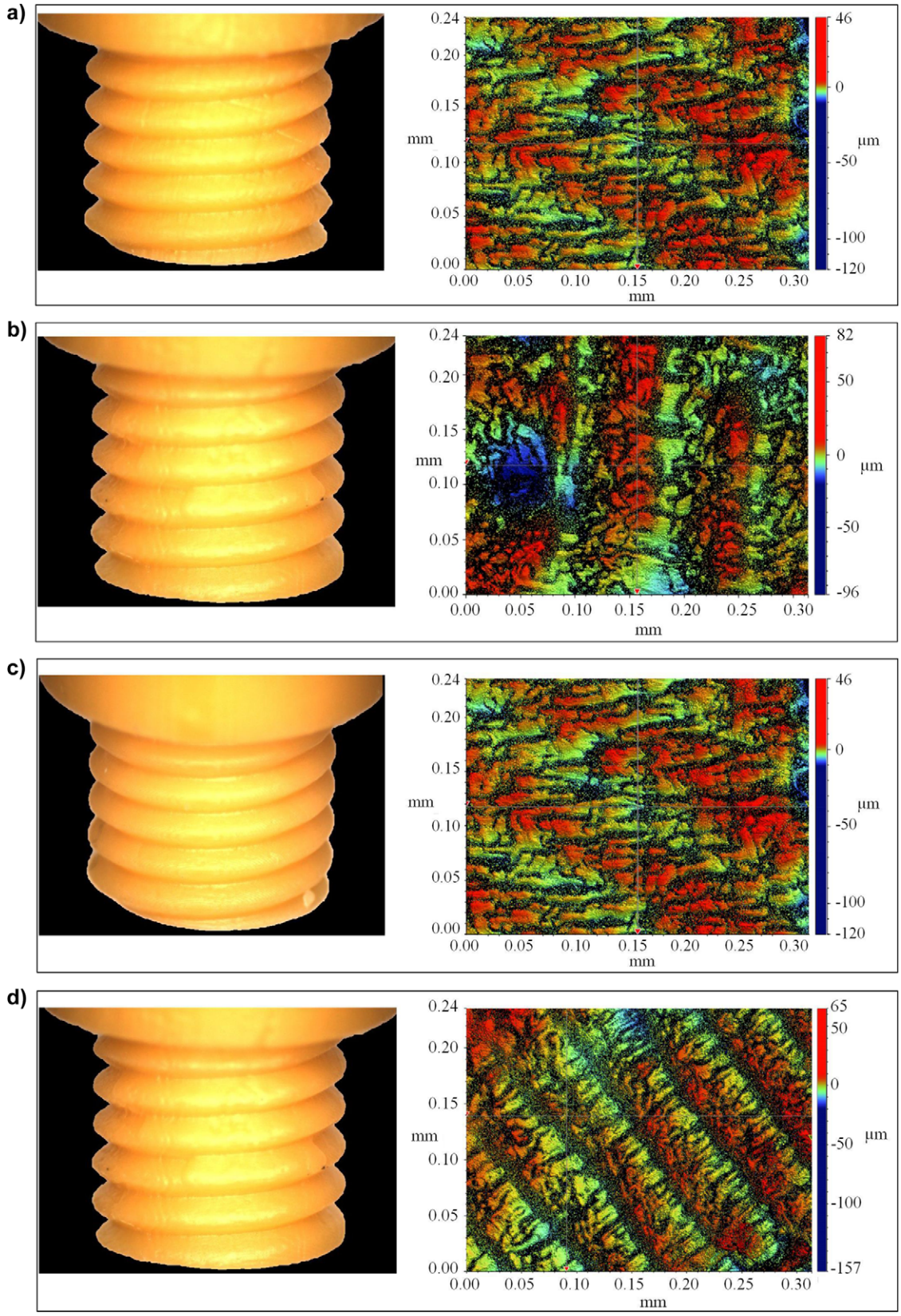

Figure 5 Product surface quality comparison. (a) Default condition; (b) different layer thickness; (c) different curing time; (d) optimized condition. mm = millimeter; μm = micron.

the surface plots regarding the factors *A*, *B*, and *D* and the total energy consumption of the process.

The measured energy consumption using the optimal combination of control parameters is 127,707.35 J. An approximate 54.16% reduction in energy consumption can be achieved compared with default working condition where the measured energy consumption is 278,707.35 J.

The optimal parameters obtained can also reduce GHG emissions attributed to the reduction of electricity consumption of the process. According to the U.S. Energy Information Administration, 1 kWh of electricity generation may incur 1.52 pounds of carbon dioxide (CO_2) emission (US EPA 2010). For a regular factory equipped with MIP SLA-based AM machines, in order to produce 3,000 parts per month, the CO_2 emission can be reduced from 414.96 pounds per month (under default condition) to 191.52 pounds per month (with optimal factors).

Product Quality Comparison

The reduction of energy consumption through adopting the optimal combination of process parameters leads to possible decay of part quality. Therefore, the part quality will be investigated and compared under different process parameter combinations. To achieve this, a Micro-Vu vision system is utilized to obtain the surface images, and a 3D optical profiler is adopted for surface roughness measurement. The comparison results are shown in figure 5. Figure 5a is the part built under default conditions (layer thickness 0.025 mm, curing time for stable layers 6 seconds, curing time transition rate 1.125 seconds per layer, and orientation 0°). It indicates good quality for the screw thread. For the part shown in figure 5b, the layer thickness is changed to 0.05 mm with all the other parameters the same as the default condition. In figure 5c, the curing time for stable layers is set to a lower level. The optimized condition is presented in figure 5d, where the layer thickness is 0.05 mm, curing time for stable layers is 4 seconds, curing time transition rate is 1.125 seconds per layer, and the orientation is 0°. R_a, the arithmetic mean surface roughness, is used to indicate different levels of surface roughness of the thread on the parts. Although the four parts are built by different combinations of process parameters, all the results of Ra are within the order of 10 μm magnitude (from 2.599 to 4.946 μm). Therefore, we can conclude that the reduction of energy consumption can be achieved without sacrificing the part surface quality.

Conclusions and Future Work

Conclusion

In this article, the mathematical model for the energy consumption of MIP SLA-based AM processes is established. Experiments are conducted and the results are analyzed to validate the proposed mathematical model. In addition, using the response surface optimization, we obtained the optimal parameters that can lead to minimized energy consumption, compared to the default parameter configuration. Significant energy saving and CO_2/GHG emission reduction can be achieved while maintaining the product quality.

Future Work

To extend this research, the presented mathematical model for energy consumption will be modified and improved so that it can include more AM processes, such as Polyjet, FDM, etc. Further, other important parts of environmental sustainability (e.g., emission, material flow, etc.) will be quantified and analyzed. In addition, in order to preliminarily explore the feasibility for batch production or mass production for AM processes, further studies will be conducted to compare the energy consumption per part and emission under different capacity utilization of the AM machine. Moreover, numerous aspects of AM processes will be explored, such as geometry complexity, part quality, etc.

Funding Information

This work is supported by the U.S. National Science Foundation under Grant number 1604825.

References

Bajpai, M., V. Shukla, and A. Kumar. 2002. Film performance and UV curing of epoxy acrylate resins. *Progress in Organic Coatings* 44(4): 271–278.

Baumers, M., P. Dickens, C. Tuck, and R. Hague. 2016. The cost of additive manufacturing: Machine productivity, economies of scale and technology-push. *Technological Forecasting and Social Change* 102: 193–201.

Baumers, M., C. Tuck, D. L. Bourell, R. Sreenivasan, and R. Hague. 2011a. Sustainability of additive manufacturing: Measuring the energy consumption of the laser sintering process. *Proceedings of the Institution of Mechanical Engineers, Part B: Journal of Engineering Manufacture* 225(12): 2228–2239.

Baumers, M., C. Tuck, R. Wildman, I. Ashcroft, and R. Hague. 2011b. Energy inputs to additive manufacturing: Does capacity utilization matter? *EOS* 1000: 30–40.

Baumers, M., C. Tuck, R. Wildman, I. Ashcroft, and R. Hague. 2017. Shape complexity and process energy consumption in electron beam melting: A case of something for nothing in additive manufacturing? *Journal of Industrial Ecology* 21(S1): S157–S167.

Burkhart, M. and J. C. Aurich. 2015. Framework to predict the environmental impact of additive manufacturing in the life cycle of a commercial vehicle. *Procedia CIRP* 29: 408–413.

Drizo, A. and J. Pegna. 2006. Environmental impacts of rapid prototyping: An overview of research to date. *Rapid Prototyping Journal* 12(2): 64–71.

Duro-Royo, J., L. Mogas-Soldevilla, and N. Oxman. 2015. Flow-based fabrication: An integrated computational workflow for design and digital additive manufacturing of multifunctional heterogeneously structured objects. *Computer-Aided Design* 69: 143–154.

EnvisionTEC. 2015. Perfactory Micro EDU. envisiontec.com/envisiontec/wp-content/uploads/MK-MCS-MicroEDU-V01-FN-EN.pdf. Accessed 11 January 2015.

Faludi, J., C. Bayley, S. Bhogal, and M. Iribarne. 2015. Comparing environmental impacts of additive manufacturing vs traditional machining via life-cycle assessment. *Rapid Prototyping Journal* 21(1): 14–33.

Gao, W., Y. Zhang, D. Ramanujan, K. Ramani, Y. Chen, C. B. Williams, C. C. L. Wang, Y. C. Shin, S. Zhang, and P. D. Zavattieri. 2015. The status, challeges, and future of additive manufacturing in engineering. *Computer-Aided Design* 69: 65–89.

Hong, C., D. Gu, D. Dai, M. Alkhayat, W. Urban, P. Yuan, S. Cao, et al. 2015. Laser additive manufacturing of ultrafine TiC particle reinforced Inconel 625 based composite parts: Tailored microstructures and enhanced performance. *Materials Science and Engineering: A* 635(21): 118–128.

Hu, K., S. Jin, and C. C. L. Wang. 2015. Support slimming for single material based additive manufacturing. *Computer-Aided Design* 65: 1–10.

Huang, S., P. Liu, A. Mokasdar, and L. Hou. 2013. Additive manufacturing and its social impact: A literature review. *International Journal of Advanced Manufacturing Technology* 67(5–8): 1191–1203.

Kellens, K., R. Renaldi, W. Dewulf, J. Kruth, and J. R. Duflou. 2014. Environmental impact modeling of selective laser sintering processes. *Rapid Prototyping Journal* 20(6): 459–470.

King, W. E., H. D. Barth, V. M. Castillo, G. F. Gallegos, J. W. Gibbs, D. E. Hahn, C. Kamath, and A. M. Rubenchik. 2014. Observation of keyhole-mode laser melting in laser powder-bed fusion additive manufacturing. *Journal of Materials Processing Technology* 214(12): 2915–2925.

Lopes, A. J., I. H. Lee, E. MacDonald, R. Quintana, and R. Wicker. 2014. Laser curing of silver-based conductive inks for in situ 3D structural electronics fabrication in stereolithography. *Journal of Materials Processing Technology* 214(9): 1935–1945.

Luo, Y., Z. Ji, M. C. Leu, and R. Caudill. 1999. Environmental performance analysis of solid freeform fabrication processes. *Proceedings of the 1999 IEEE International Symposium on Electronics and the Environment*. DOI: 10.1109/ISEE.1999.765837.

Martukanitz, R., P. Michaleris, T. Palmer, T. DebRoy, Z. K. Liu, R. Otis, T. W. Heo, and L. Q. Chen. 2014. Toward an integrated computational system for describing the additive manufacturing process for metallic materials. *Additive Manufacturing* 1–4: 52–63.

Meteyer, S., X. Xu, N. Perry, and Y. F. Zhao. 2014. Energy and material flow analysis of binder-jetting additive manufacturing processes. *Procedia CIRP* 15: 19–25.

Mitteramskogler, G., R. Gmeiner, R. Felzmann, S. Gruber, C. Hofstetter, J. Stampfl, J. Ebert, W. Wachter, and J. Laubersheimer. 2014. Light curing strategies for lithography-based additive manufacturing of customized ceramics. *Additive Manufacturing* 1–4: 110–118.

Mognol, P., D. Lepicart, and N. Perry. 2006. Rapid prototyping: energy and environment in the spotlight. *Rapid Prototyping Journal* 12(1): 26–34.

Montgomery, D. C. 2012. *Design and analysis of experiments*, 8th ed. New York: John Wiley & Sons.

Pan, Y., C. Zhou, and Y. Chen. 2012. A fast mask projection stereolithography process for fabricating digital models in minutes. *Journal of Manufacturing Science and Engineering* 134(5): 051011.

Park, S.-I., D. W. Rosen, S.-K. Choi, and C. E. Duty. 2014. Effective mechanical properties of lattice material fabricated by material extrusion additive manufacturing. *Additive Manufacturing* 1–4: 12–23.

Prasanna Kumar, C. S., S. P. Sabberwal, and A. K. Mukharji. 1995. Power factor measurement and correction techniques. *Electric Power Systems Research* 32(2): 141–143.

Reeves, P. 2009. *Additive manufacturing—A supply chain wide response to economic uncertainty and environmental sustainability*. Wirksworth, UK: Econolyst Limited.

Short, D. B., A. Sirinterlikci, P. Badger, and B. Artieri. 2015. Environmental, health, and safety issues in rapid prototyping. *Rapid Prototyping Journal* 21(1): 105–110.

Sreenivasan, R. and D. Bourell. 2009. Sustainability study in selective laser sintering—An energy perspective. In Proceedings of the 20th Solid Freeform Fabrication Symposium, 3–5 August, Austin, TX, USA.

Stratasys. 2015. NASA's human-supporting rover has FDM parts. www.stratasys.com/resources/case-studies/aerospace/nasa-mars-rover. Accessed 11 November 2016.

Telenko, C. and C. Conner Seepersad. 2012. A comparison of the energy efficiency of selective laser sintering and injection molding of nylon parts. *Rapid Prototyping Journal* 18(6): 472–481.

US EPA (U.S. Environmental Protection Agency). 2010. Annual non-basedload CO2 output emission rate, year 2010 data. www.epa.gov/cleanenergy/energy-resources/refs.html. Accessed 4 January 2016.

Weller, C., R. Kleer, and F. T. Piller. 2015. Economic implications of 3D printing: Market structure models in light of additive manufacturing revisited. *International Journal of Production Economics* 164: 43–56.

Wohlers. 2016. Wohlers report 2016 published: Additive manufacturing industry surpassed $5.1 billion. http://wohlersassociates.com/press71.html. Accessed 11 November 2016.

Wohlers, T. 2013. The future of additive manufacturing. *Wohlers Associates*. http://wohlersassociates.com/blog/2013/09/the-future-of-additive-manufacturing/. Accessed 11 November 2016.

Wong, K. V. and A. Hernandez. 2012. A review of additive manufacturing. *ISRN Mechanical Engineering*. DOI: 10.5402/2012/208760.

Xu, X., S. Meteyer, N. Perry, and Y. F. Zhao. 2015. Energy consumption model of Binder-jetting additive manufacturing processes. *International Journal of Production Research* 53(23): 7005–7015.

Yang, N., Y. Tian, and D. Zhang. 2015a. Novel real function based method to construct heterogeneous porous scaffolds and additive manufacturing for use in medical engineering. *Medical Engineering & Physics* 37(11): 1037–1046.

Yang, S., Y. Tang, and Y. F. Zhao. 2015b. A new part consolidation method to embrace the design freedom of additive manufacturing. *Journal of Manufacturing Processes* 20(3): 444–449.

Zha, W. and S. Anand. 2015. Geometric approaches to input file modification for part quality improvement in additive manufacturing. *Journal of Manufacturing Processes* 20(3): 465–477.